WFC3 Instrument Science Report 2010-15

Boosting Count-rates with Earth Limb Light and the WFC3/IR Count-rate Non-linearity

A. G. Riess and L. Petro
October 22, 2010

ABSTRACT: We report the results from the CAL/WFC3 program 11933 to constrain the effect of count-rate non-linearity on the WFC3/IR detector by observing stars in NGC 1850 with and without superposed scattered Earth light. The scattered Earth light raises the apparent count rate of the stars by a measurable amount, allowing us to measure its impact on photometry. After accounting for a time varying sky level we find a small effect at the level expected, about a 1% decrease in measured count rate per factor of 10 reduction in the true count rate. The precision of the measurement is limited by the maximum Earth light at the minimum bright Earth limb angle allowable under FGS guiding, ~2-4 electrons/sec/pixel, 2 to 3 orders of magnitude less than the lamp used on NICMOS for the same purpose.

Introduction

Count-rate non-linearity (hereafter CRNL) also known as reciprocity failure is particularly problematic for HgCdTe detectors in the low background environment of space. Similar detectors used from the ground are flooded with backgrounds 1000s times higher than HST and thus the dynamic range of the apparent count rates of sources and calibration targets is greatly reduced and with it the problem of count-rate non-linearity. Past work has shown the effect on NICMOS (Bohlin, Lindler, Riess 2005) ranged from a 6% to 10% loss in measured flux per factor of ten decrease in flux in F110W for Camera 2 and 1, respectively. The non-linearity diminished toward the red, reaching 3% for Camera 2 for F160W. For typical, faint science sources (i.e., below the sky) the net effect was quite large because photometry zeropoints are established from stars that are 10 magnitudes or 4 dex brighter. Thus the net effect on the faint end of science photometry (i.e., sky-dominated) in the blue is 0.2 to 0.4 mag when using the extrapolation from zeropoint calibration to the sky flux.

This calibration for NICMOS was obtained on-orbit in a direct manner; through the measured difference between source and source plus background light. That the same sources vary (as a power law) in their apparent count rate in the presence of additional lamp light indicates that the critical detector parameter is the rate, not the integrated signal or signal history and has been

explained to result from charge trapping (Smith et al. 2007).

For WFC3/IR, CRNL is expected to be much smaller than for NICMOS due to improvements in the detector manufacturing and optimization of their operating conditions which has boosted their quantum efficiency, reduced pixel defects, and decreased charge trapping. Initial measurement (Riess 2010) has borne out this expectation. By comparing the photometry of star clusters observed over a wide dynamic range and at overlapping wavelengths in WFC3/IR and NICMOS and/or ACS-WFC, we found a significant detection of a non-linearity in WFC3/IR photometry which is in the same direction but a few times smaller than that of NICMOS. From the stars we measured a non-linearity of WFC3/IR of 1% per dex over a range of 10 magnitudes (4 dex) with no apparent wavelength dependence. The impact of this non-linearity is that photometry of faint (i.e., sky dominated) sources calibrated with WFC3/IR zeropoints will appear 0.04 +/-0.01 mag too faint.

Because the problem of CRNL was not detected in NICMOS until late in the development cycle of WFC3, a similar lamp assembly with the ability to add flux to an external measurement was not included in the WFC3 IR channel. However, during Cycle 17, we produced a varying count-rate on the WFC3 IR detector while observing a star cluster graze the bright limb of the Earth under near-CVZ-like conditions. Thus, we varied the incident sky flux accompanying stellar sources between the day and night side of the orbit (CAL/WFC3 11933).

Observation Plan

The goal of our observation is to observe a star cluster continuously over the course of an HST orbit while the telescope line of sight (LOS) moves from near-Earth occultation to the unocculted side of the orbit. During near-Earth occultation, HST would observe the target superposed with scattered Earth limb light, increasing the count-rate of stars by a measurable amount, the amount seen in an annulus around each star. Differences in the sky-subtracted photometry due to varying stars' count rates can be used to measure the CRNL much as a lamp was used to calibrate the effect on NICMOS. The virtue of this approach is that it is independent of any astrophysical knowledge of the sources—it is a purely differential measurement. However the level of added background is limited by the minimum angle to the bright Earth limb at which HST can observe, 13.5 degrees, before HST switches from FGS to gyro guiding (a limit that anticipates an inability to maintain FGS lock in the presence of extremely bright sky). Based on experience with other HST instruments, we expected the maximum sky level to reach ~5-10 electrons/sec/pixel (Earth weather dependent), significantly higher than the more typical 0.5 electrons/sec/pixel, but far lower than the few thousand electrons/sec/pixel attainable with the NICMOS lamps. For comparison, a background of 5 electrons/sec/pixel would be the mean count rate for the central 10 pixels of a ~20th mag star (F160W, Vega system). Thus, increasing the stellar count rate by an order of magnitude or more from Earth limb light will only occur for stars of ~22.5 mag or fainter. In the ~5 minute interval of maximal Earth light the expected signal-to-noise ratio (SNR) is ~20 without additional light or ~20*sqrt(10)~60 in the presence of 10 times more background. Because we expect photometric changes for such stars due to CRNL to be ~1%, a significant detection of the CRNL would require a SNR of ~300 for any individual star, far higher than we will achieve. The solution is to average the results from 1000's of stars in the hope of reaching a significant measurement of CRNL.

Our first opportunity to measure the CRNL occurred for the star cluster NGC 1850 ([α, δ] = [77.17°, -68.43°]; [λ, β] = [333.3°, -84.8°]). We observed it in 2 single-orbit visits, one (Visit 02) with F160W on 07/23/10 (DOY 204) and the other (Visit 01) in F110W on 07/27/10 (DOY 208). Each orbit consisted of a continuous set of SPARS50, NSAMP=7 reads. A stack of images before and after Earth illumination is shown on the left of Figure 1 and a single exposure with maximum Earth light on the right.

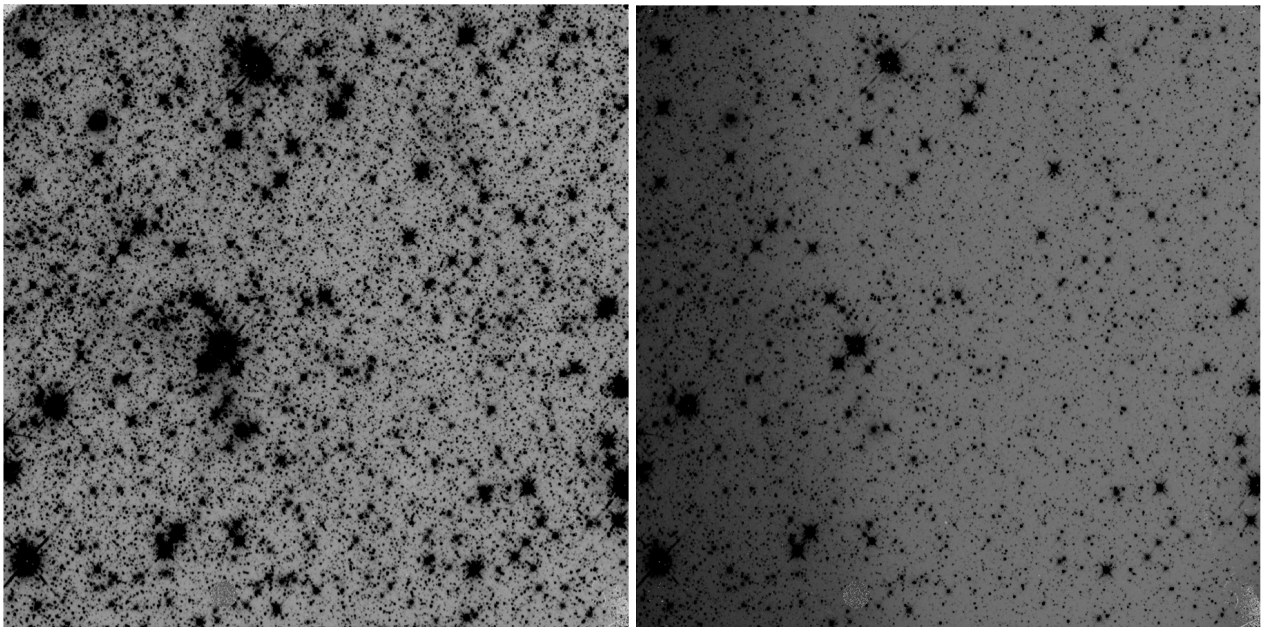

Figure 1: NGC 1850, stack of exposures without Earth light on left, single exposure with maximum Earth light on right. Note the characteristic vertical band of stray light on the left hand side, as noted by Hilbert and McCullough (2009).

Orbit

Opportunities to observe NGC 1850 under the conditions that we require, namely with the LOS grazing the bright Earth limb, happen only a few, brief times each year. The constraints that so limit these observations are illustrated in Figure 2. First, because HST's orbital plane regresses with a sidereal period of 55.0 day, the angle between the LOS to a CVZ, or near-CVZ target and the pole of the HST orbit, $\theta_{T\text{-}OP}$, varies with that same regression period as given by $\cos \theta_{T\text{-}OP} = \cos i \sin \delta_T + \sin i \cos \delta_T \sin(\alpha_{AN} - \alpha_T)$, where the target orbital co-latitude is $\theta_{T\text{-}OP}$, the target celestial declination and right ascension are δ_T and α_T, the inclination of the orbit pole from the celestial pole is i, and the celestial right ascension of the orbit plane ascending node is α_{AN}. In Figure 2, the light black line represents the variation of $\theta_{T\text{-}OP}$.

Furthermore, the angle between the LOS to NGC 1850 and the orbit pole varies around the HST orbit and reaches a minimum once per orbit. The minimum limb angle during a target visibility within an HST orbit ($\theta_{limb} = 90^\circ - \theta_{Earth} - \theta_{T\text{-}OP}$, where θ_{Earth} is the semi-angle subtended Earth at HST) varies between 0° and 17° with a 55-day period, as illustrated in Figure 2 by the heavy black line. Six times each year for an interval of 2 weeks the LOS to NGC 1850 skims Earth's limb once during each HST orbit. It is one of these intervals that was chosen for the observations presented here. That selection was made in order that the limb was illuminated by sunlight when the LOS

skimmed the limb. To approximately meet that condition, the right ascensions of the Sun, NGC1850, and the southern orbit pole were required to be equal. The difference in right ascension of the target and the Sun is shown as a heavy red line in Figure 2, and the difference of the target and the southern orbit pole is shown as a dotted red line in Figure 2. The desired equality is reached on DOY 200, which favors the two LOS skimming intervals centered at DOY 206. Additional considerations in the scheduling were to avoid SAA-impacted orbits and to specifically select a time when the minimum target limb angle was approximately equal to the minimum allowed angle for FGS guiding. All these constraints were satisfied on DOY 204 and DOY 208.

Performance

The observing conditions achieved as a result of the planning described in the preceding paragraph are presented in Figure 3. The left-hand panel of Figure 3 presents the limb angle of the LOS as a function of exposure start time from the start of the single-orbit visits on July 23 (V02) and 27 (V01). The minimum limb angle was 13.5˚ on July 23 (DOY 204) and 15.0˚ on July 27 (DOY 208), in approximate agreement with the planned angles. The brightness of the bright Earth stray light on the WFC3/IR detector as a function of time elapsed from the beginning of the visit is presented in the middle panel. At the beginning and end of each visit the signal rates are low, 1.0 electrons/sec/pixel in F160W (DOY 204) and 1.9 electrons/sec/pixel in F110W (DOY 208). The peak rates of the sky + bright Earth are 5.0 electrons/sec/pixel and 3.8 electrons/sec/pixel,

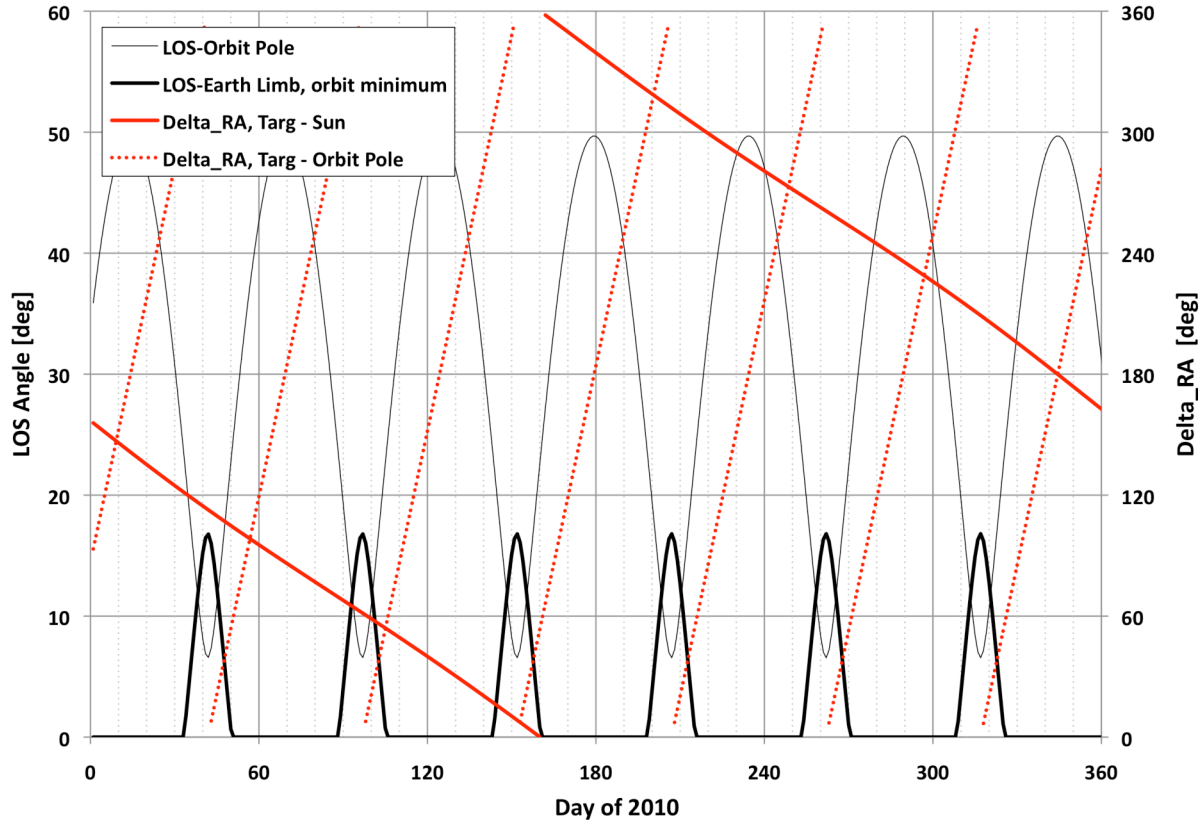

Figure 2: Variation of the orbital circumstance of the LOS to NGC 1850. The plotted quantities are described in the text. Because NGC 1850 is near the southern orbital pole, it is that pole referenced here.

respectively. The time of peak signal rate is in agreement with the time of minimum LOS limb angle. Of concern was whether FGS tracking would be affected by the increased stray light and thereby would possibly reduce the accuracy of the aperture photometry. The jitter of the FGS measurements of the positions of the guide stars during each visit (the radial r.m.s. of the position) is shown as a function of limb angle in the right-hand panel of Figure 3. The jitter during both visits is generally 3.9 mas, which is consistent with the typical performance of the FGS, 1 – 3 mas. It is noteworthy that no losses of FGS guide star lock occurred. Also, two limited discrepancies are noteworthy. First, a single exposure suffered from approximately twice the general jitter, to 7 mas. Second, the jitter on DOY 204 increased perceptibly for four exposures at the limb. The peak r.m.s. was 5.3 mas at 16°. Because the jitter for all the exposures is less than 7 mas worst case, the jitter does not significantly affect aperture photometry from the 128-mas WFC3/IR pixels.

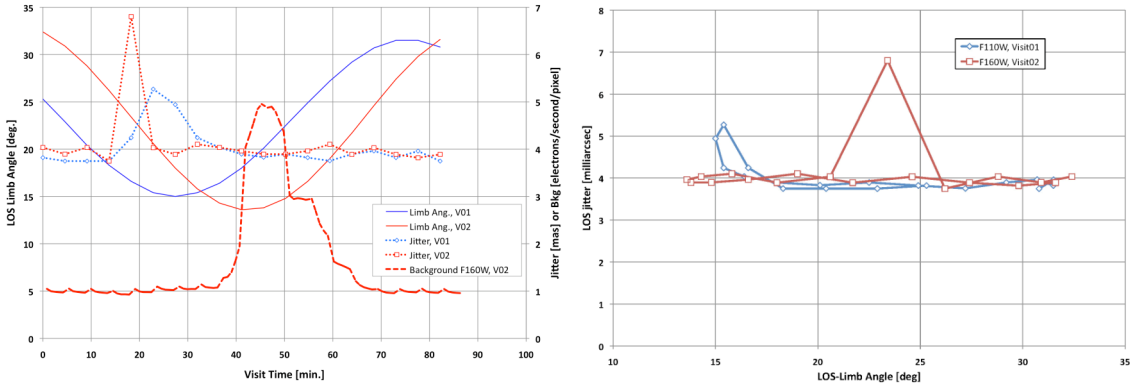

Figure 3: Observing conditions achieved for CAL/WFC3 11933 V01 and V02. The limb angle at the middle of each exposure, the median sky brightness of each exposure of the second visit, and the jitter of the FGS-measured GS position are presented in the left-hand panel. In the right-hand panel, the r.m.s. jitter of the measured positon of the guide star images in the FGSs during each exposure is presented as a function of the limb angle of that exposure.

Systematic Error Sources

We considered the possibility that the Earth's atmosphere at HST's altitude could affect the signal, position, or PSF of the stellar images. This possibility is suggested by the geometry of the LOS grazing Earth's limb, which provides an atypically long slant range through Earth's atmosphere, a path that dips into denser atmosphere below the HST orbit, and the large scale height of Earth's atmosphere at HST's orbit (~90 km). However, upon evaluating those possibilities, we find that column density along the LOS for the reported exposures is so small that it cannot have any of the feared effects. The minimum height of the LOS (the "impact parameter") is $h_{min} = r_{min} - R_{Earth} = a_{HST} \sin(\theta_{Earth} - \theta_{Limb}) - R_{Earth}$, where the values $R_{Earth} = 6371$ km , $a_{HST} = 6940$ km, $\theta_{Earth} = 66.64^{\circ}$, and $\theta_{Limb} = 13.5^{\circ}$ are adopted for the circumstances of our exposures. The minimum height along the LOS is shown as a function of θ_{Limb} in Figure 4. For $\theta_{Limb} = 13.5^{\circ}$, the minimum height is 466 km, considerably below HST's altitude at the time of our exposures, 569 km.

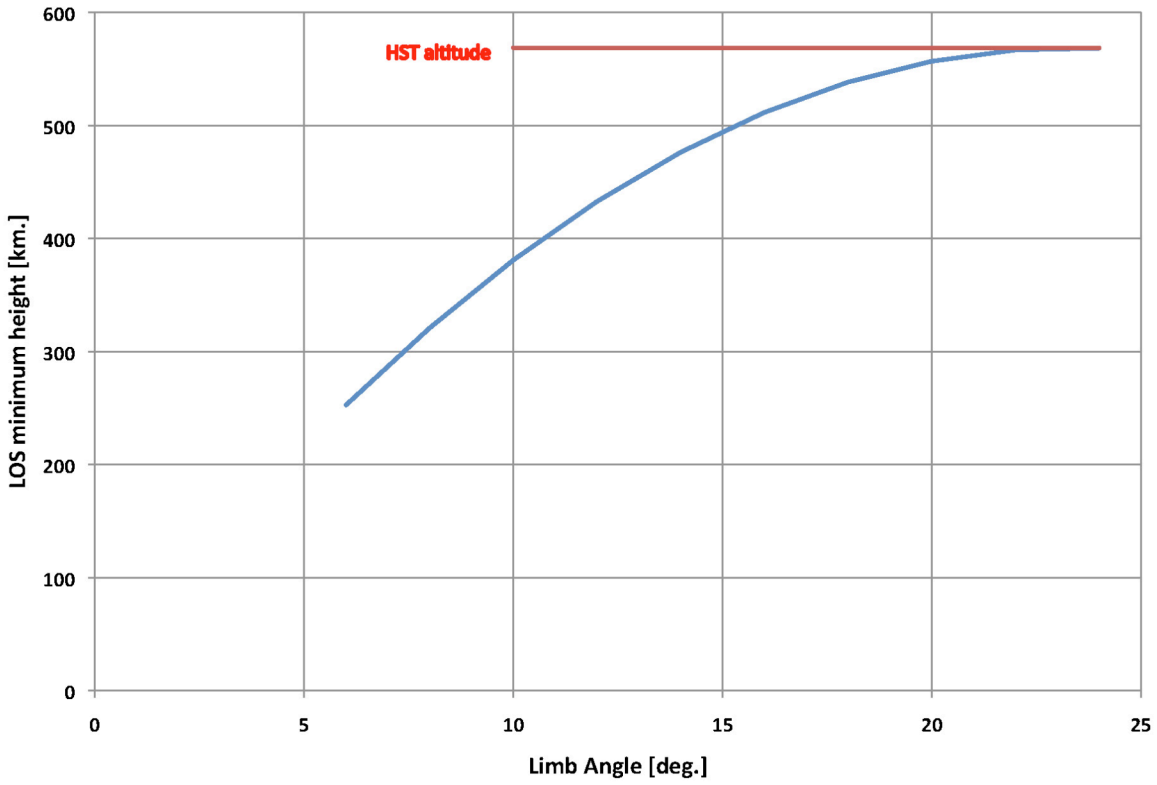

Figure 4. Minimum LOS height.

The cumulative column density along our worst-case LOS, θ_{Limb} = 13.5°, is shown as a function of the slant range in Figure 5. Also shown, is the height of the LOS as a function of the slant range. The column density along the LOS is 7.4×10^{20} m^{-2}. From Earth's surface, the zenith column density is 6.6×10^{29} m^{-2}, so our worst-case LOS column density corresponds to air mass X = 1.1×10^{-9}, which will have negligible effect on the radiometric signal, image position, or image PSF.

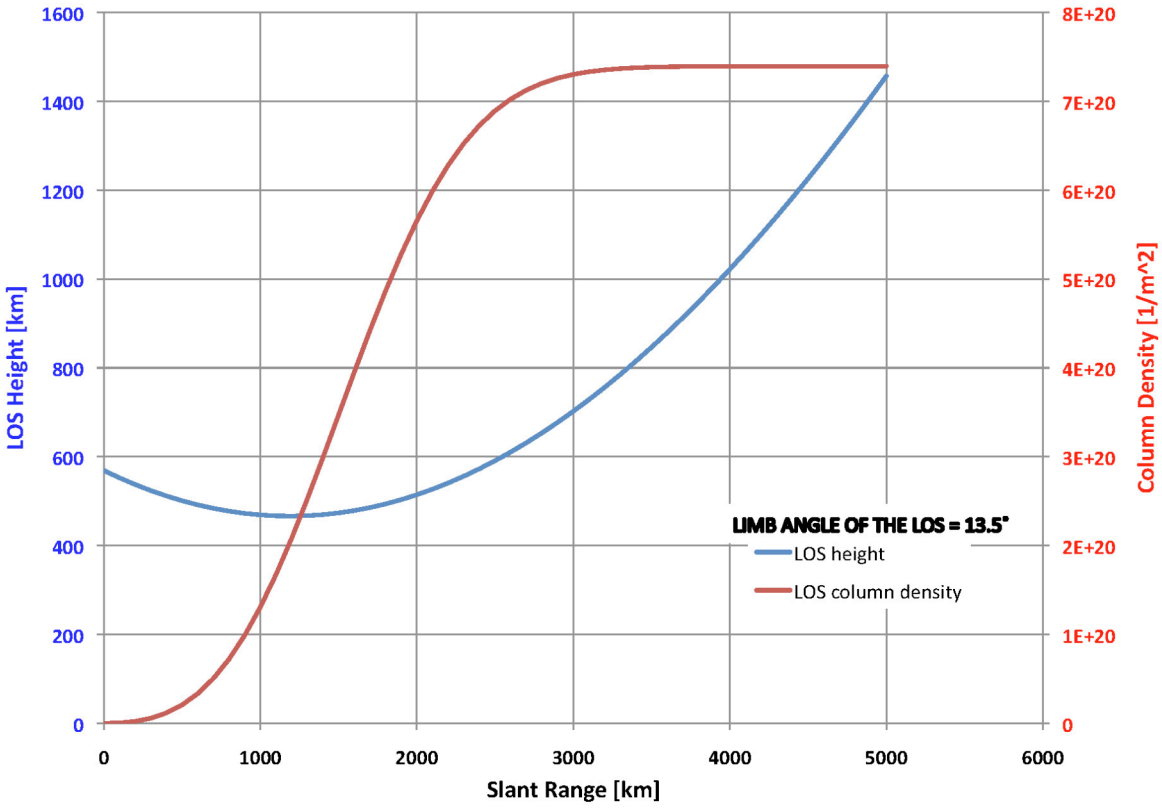

Figure 5. Column density along the NGC 1850 LOS. The worst-case limb angle, 13.5°, is adopted and the cumulative column density is shown in red as a function of the slant range. Also shown in blue is the height above Earth of the LOS.

Analysis

Up-the Ramp

Up-the-ramp-sampling (i.e., samplings of counts versus time) to reject cosmic rays is an early step in the calibration process of WFC3/IR data (Fixen et al 2000). This process assumes that the count rate of a pixel is constant and identifies cosmic rays by deviations from constancy. In the presence of changing background, such as occurs in our observations (as seen in Figures 3 and 6), the ramp will measure a mean level sufficient for photometry. That is a constant source pixel plus a varying sky level will result in a constant source pixel plus a mean sky level after application of the software ramp. A pure sky pixel will result in the same mean sky level as included for a source pixel, and the difference used to measure photometry will be preserved. However, the cosmic ray clipping that occurs during the measurement of the count ramp can cause biases in the presence of

varying sky. Cosmic rays occurring early or late in the ramp will cause the count-rate to be measured from the other end of the ramp when the sky level was different than the mean. The result will appear as an increment or decrement (i.e., over or under rejected cosmic rays). More problematic is the possibility that the ends of the ramp may appear to change too rapidly (due to the changing sky) even without cosmic rays occurring and may be rejected from the ramp. This can bias those pixels away from the mean sky level. As this bias may not be the same for source and pure sky pixels (due to the differences in their Poisson noise), the result can be biased photometry. To test for inaccurate rejections along the ramp we measured the fraction of pixels that retained all 7 samples of the ramp over the course of the observations, i.e., as the sky level changed. Assuming the cosmic ray rate is unchanged throughout the orbit, we saw this fraction change from 98.6% in the absence of added or changing background to 75% at the peak of the additional background, clear evidence of excessive rejection. To mitigate the problem we increased the value of sigma (keyword *crsigmas* in the *crrejtab* used by *calwf3*) from 4 to 8 resulting in a constant fraction of 98.6% with a dispersion of 0.05% (i.e., 1.4% of pixels with one or more CRs rejected) throughout the observations.

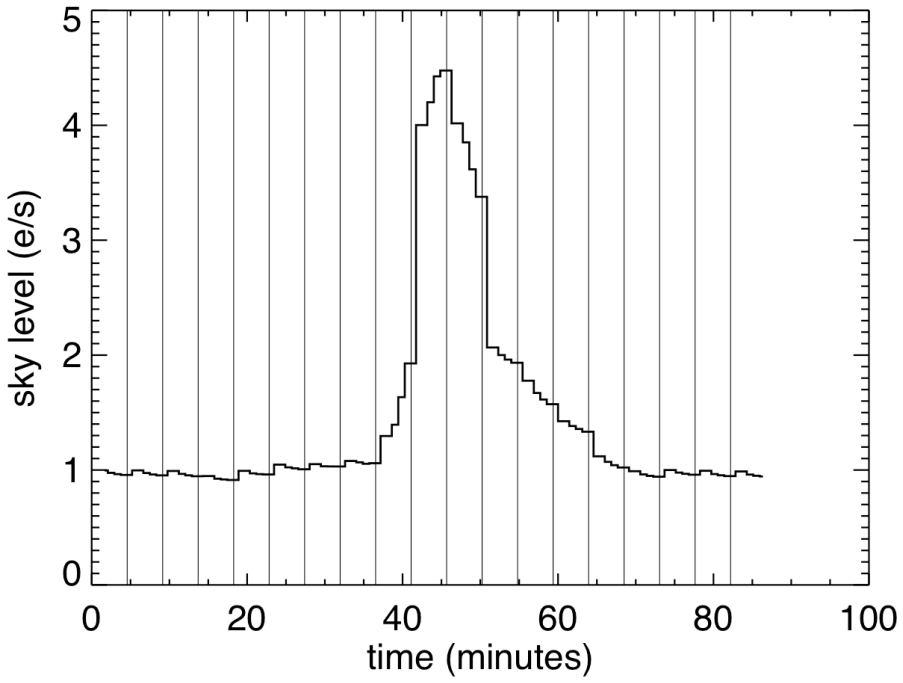

Figure 6: Median Sky level in visit 2, 10933 in F160W during orbit. Vertical lines shown end of each exposure with data values plotted at each sample. As shown, near the maximum Earth light the sky level is changing rapidly during a exposure requiring us to relax the cosmic ray rejection to avoid rejecting clean sky pixels and biasing pixel values.

Sky level

Because the fields are relatively crowded and because the added Earth light is non-uniform, great care was required in measuring the local sky level at each star. However, because the CRNL depends only on changes to *relative* photometry with changing count-rate, the problem of accounting for the sky level can be simplified. We can assume that a source pixel is the sum of 3 components; 1) a constant count rate from the source 2) a constant count rate from the static sky and 3) excess sky due to the bright Earth. The static sky is assumed to be composed of features in the direction of the source e.g., faint companion sources, astronomical nebulosity, OTA stray light from astronomical sources, etc., all of which do not change with time. This would be the hardest part of the sky to measure accurately but in the determination of CRNL, its presence in *both* the images with and without added sky light means it largely cancels out of the measurement[1]. Rather we must account only for the addition of component 3) on the unseparated sum of components 1) and 2). To do this we produced a mean image from all exposures without added Earth light, i.e., from the beginning and ends of the orbit when the LOS is far from the bright Earth. This mean image was then subtracted from every frame to produce an image composed purely of component 3), the excess sky. A local annulus of inner radius 10 pixels, outer radius 15 pixels was used to determine the excess sky to subtract from the source pixels. The mean image was also used to produce a master list of stellar sources using the *daofind* algorithm, down to a few sigma of the noise. The total number of such sources was 9000 in the F160W frame and 7200 in the F110W frame.

Photometry

Although no dithering occurred during each orbit and FGS lock was maintained, we measured the size of any global shift for each frame to improve the precision of our photometry. These global shifts were small as expected, never rising above 0.04 pixels for any axis. The global shifts were used to identify the centers of sources in each frame. Photometry for each source in the master list for each frame was then measured using small apertures of radius 2 pixels using the excess sky measured in the annuli as described in the previous section. Data quality flags in the flt frames were employed to reject any sources with a flagged pixel inside the aperture. We note that although all measurements were made using round apertures and annuli in the distorted flt frames, all measurements are differential with respect to sources in the same position of the frame and thus geometric distortion is not relevant to our subsequent analysis.

To verify the accuracy of our excess sky measurements and our photometry we measured the 2nd moment of the mean excess sky-subtracted PSFs throughout the orbit. Because the 2nd moment is sensitive to the presence of excess light (i.e., the first moment) or changes in the PSF width, this is an important test of the fidelity of our small aperture photometry. As tabulated in Figure 7 and 8, it is constant.

In Figures 7, 8 and 9 we show the photometry of each frame relative to a fiducial frame, whose choice is arbitrary but was chosen as the 4th in the sequence which occurs before the onset of

[1] The cancellation of the static sky is not perfect because its superposition with the Earth light is raised to a power, α, by CRNL as described in the next section, i.e. (static+Earth)$^{\alpha}$ - static$^{\alpha} \neq$ Earth$^{\alpha}$ requiring us to account for this in the model.

scattered Earth light. Each panel plots the mean count rate of the stellar pixels in the small apertures versus the fractional change in photometry between the frame and the fiducial frame. To improve the statistics we then bin the individual stellar photometry into 20 bins (logarithmically stepped) of count rate using the mean of the bin after iterative 3 sigma clipping to exclude outliers (transient hot pixels and the like). It is possible that there may still be small frame-to-frame variations in the PSF width resulting from telescope breathing which could affect the integrated flux in a small aperture. We account for such frame-to-frame deviations (i.e., aperture corrections) from the highest count rate bins where the impact of CRNL would be less than 0.1% or >10 times smaller than the lower count rate bins. This was measured from the mean of the 4 highest count rate bins and subtracted from each bin. These frame-to-frame deviations are small, typically a few tenths of a millimag which is an order of magnitude smaller than the scale of the CRNL. They are also constant for an exposure unlike the CRNL.

Modeling the Data

Predicting the results for an unknown value of the exponent of the power law, α, requires a bit of manipulation due to the fact that *we observe count rates that have already been affected by the CRNL*. In addition, we have measured photometry by separating the components of the observed count rate and so care must be taken in using equation (1) to apply the model to the data.

To measure the CRNL we assume the functional form found in NICMOS (de Jong et al. (2006)) and the Goddard DCL tests of similar detectors to WFC3/IR,

$$cr=flux^{\alpha} \quad (1)$$

where cr is the observed count rate for a pixel and flux is the flux incident on the pixel.

Here following equation (1) we define the relevant apparent count rates and incident fluxes as:

$$\text{Source: } 1=1*\alpha \quad (2)$$

$$\text{Static Sky: } 2=2*\alpha$$

$$\text{Earth-limb Sky: } 3=3*\alpha$$

where the terms 1*, 2*, and 3* are the corresponding fluxes and 1,2,3 are the count rates.

When we measure the photometry of a source and the underlying static sky before or after the onset of scattered Earth light (referred to as the "Off" frame here and in Figures 7 and 8) we have measured the quantity $Off=(1*+2*)^{\alpha}$. When we measured the source photometry with Earth-limb light "On" we have measured: $On=(1*+2*+3*)^{\alpha} - E_{cr}$ where E_{cr} is the light in the annuli around sources measured from the template subtracted frame with Earth light described in the **Sky Level** section. Now, the annuli around sources are assumed to have 1=1*=0. So when we measured the excess sky in the annuli of the template image-subtracted that annulus measured the Earth-limb annulus count rate:

$$Ecr=(2*+3*)\alpha - 2*\alpha. \quad (3)$$

Our best estimate of the Earth-limb flux is then given by

$$3*=(Ecr+2)1/\alpha - 21/\alpha \quad (4)$$

where 2 is given as the mean count rate of the sky in the stack of images without Earth light.

Finally, we can use the model to *predict* the photometry from a frame with Earth-limb light in terms of the Off photometry and Earth-limb sky flux as

$$On=(1^*+2^*+3^*)\alpha - Ecr =(Off1/\alpha+3^*)\alpha - ((21/\alpha+3^*)\alpha-2) \quad (5)$$

Whose equality can be verified by substitution from equations (2)-(4) and the definition of Off .

And so for an assumed value of Off and the determination of the Earth light 3* via equation (3) and (4) for a specific frame we can predict the value of the On photometry from equation (5) and compare it to what we observed to constrain α. This is shown in Figures 7 and 8 as a blue line.

As shown in Figures 7 and 8 we find the value of α determined from a χ^2 minimization to be in good agreement with the value expected from Riess (2010) though with about half the precision. Specifically we find α=1.004 +/- 0.002 or Δmag/dex of 0.01 +/- 0.005 for each filter.

We had some concern that the spatially non-uniform illumination of the frame by Earth light (see Figure 1, right hand panel), in some cases as much as 75% increase of the mean sky, could be adding excess variance to our measurements because the Earth light we assume was taken to be the average across the frame. To test for this we divided each frame along a vertical line one quarter of the way across the frame from the x=0 line (see Figure 1, right panel) which divides the frame across the strong gradient of Earth light. Analyzing each portion separately then combining the results gave nearly identical results (well under the standard error), demonstrating that the non-uniformity has little impact on our analysis.

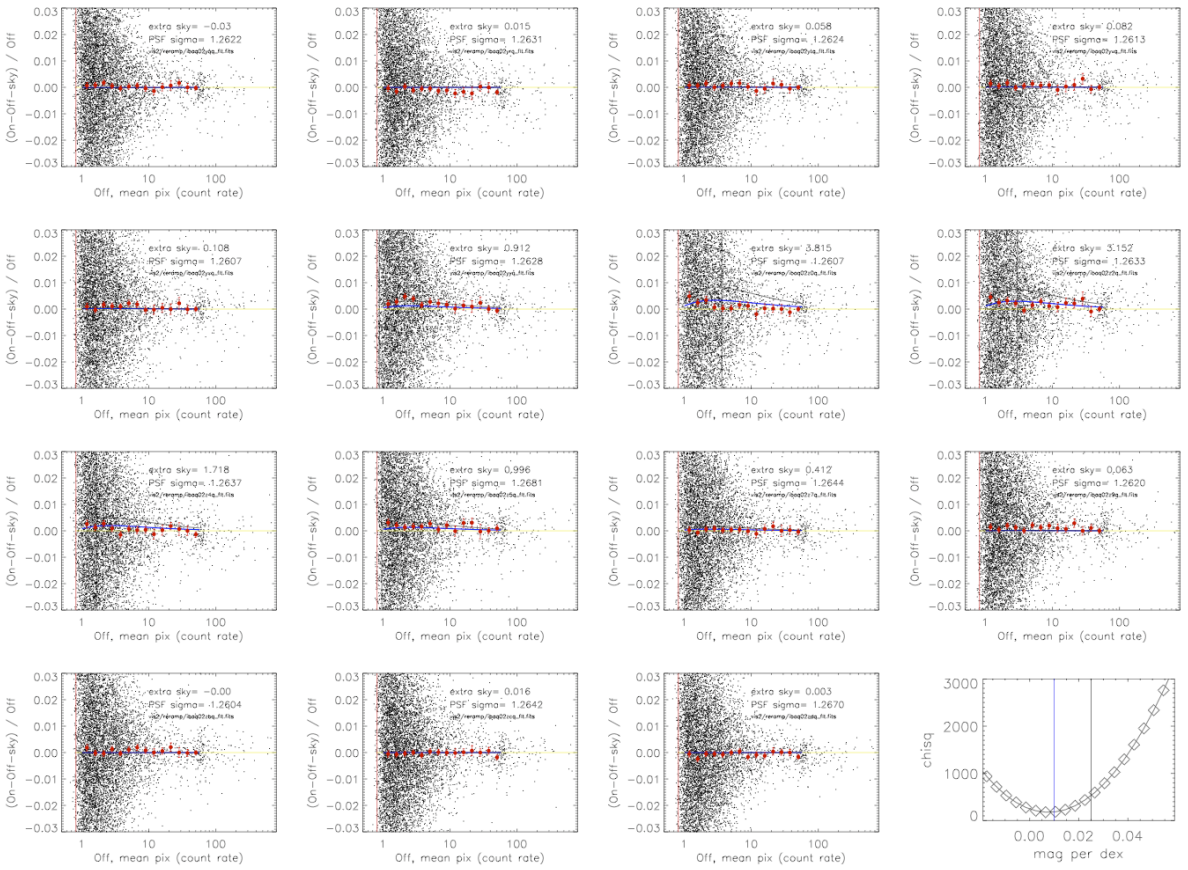

Figure 7: Photometric differences for sources observed with and without the addition of Earth limb light. Each dark point shows the mean pixel value for a stellar source measured with the F160W filter with a small aperture. The x-axis shows the mean pixel count rate without Earth light and the y-axis shows the fractional change in the photometry of sources with and without Earth light. In the absence of CRNL, the difference should be zero. Red points are binned averages. The thin blue line shows the expectation for a CRNL corresponding to α=0.004, the level measured by cross-instrument calibration. The dark line shows the high level of CRNL as would be expected for NICMOS. Each panel shows a different exposure in the sequence with the extra sky from the Earth limb and the measured, mean PSF width given. The lower right panel shows a χ^2 minimization to determine the best estimate of α for the combined dataset. The vertical blue line shows the expected CRNL for WFC3 and the vertical dark line the level expected for NICMOS.

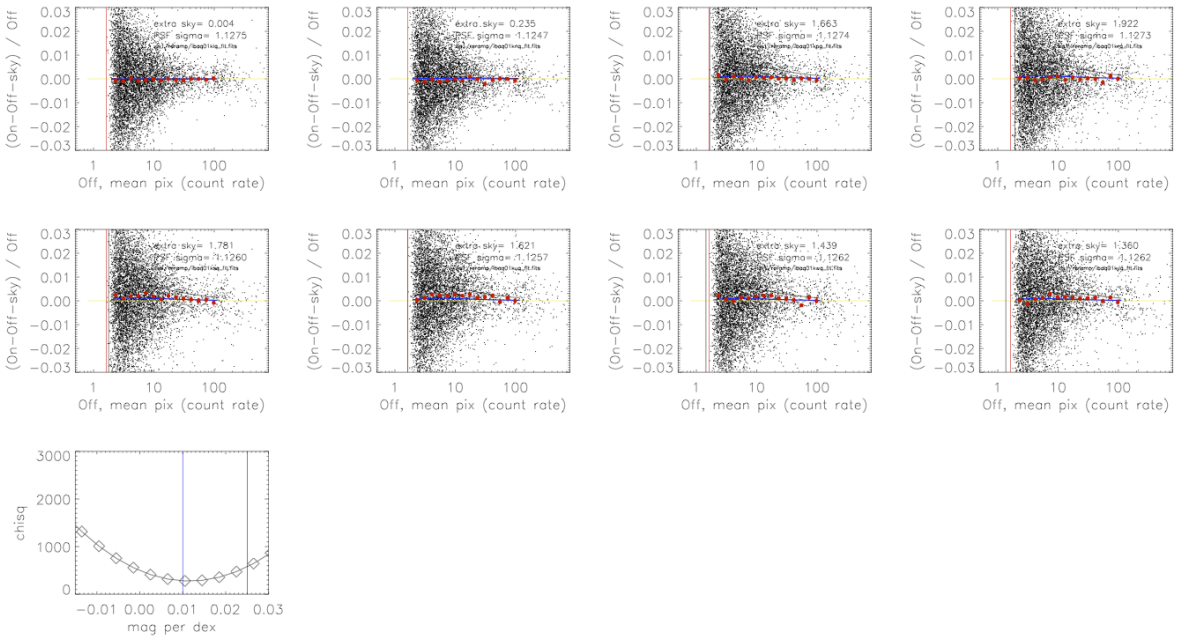

Figure 8: Same as Figure 7 but for F110W.

Discussion

While the results we have found are consistent with previous results for the CRNL from Riess (2010) the precision at best (i.e., if there are not additional systematics involved) is half as good. The main shortcoming of our use of Earth light to calibrate the WFC3/IR CRNL is that the maximum Earth light we achieved under FGS guiding is too low. Ideally we would be adding 1000s of electrons/sec/pixel as occurs with the NICMOS lamps which would result in a 2% to 3% deviation, i.e., near the top of the plots in Figures 7, 8, 9 . Even just 200 electrons/sec/pixel of background would cause a 1.5% deviation which would provide a strong calibration. At 20 electrons/sec/pixel the expected deviation would match the level shown for F160W for the NICMOS CRNL, i.e., α=1.01. The silver lining here is that the CRNL for WFC3/IR is apparently quite low, much lower than it was for NICMOS, but so low that its pretty hard to measure to even greater significance.

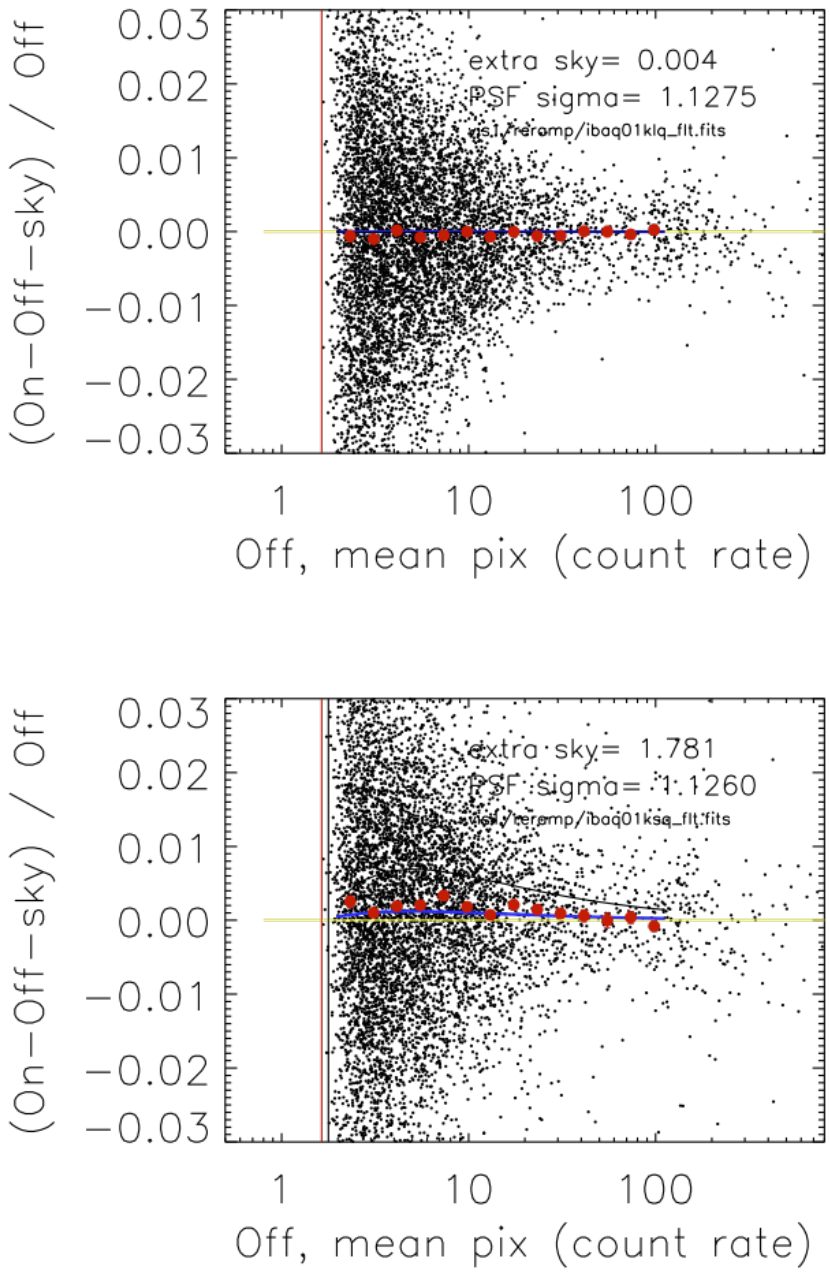

Figure 9: Same as Figure 8 but showing more detail for 2 example panels with and without Earth light.

Acknowledgments

We express thanks to members of the WFC3 Team at STScI and Goddard for helpful discussions, to William Januszewski and Merle Reinhart for scheduling these observations, and to Howard Bushouse for his review of this ISR..

References

Bohlin, R., Lindler, D., and Riess, A, 2005, NICMOS ISR 2005-002, "Grism Sensitivities and Apparent Non-linearity"

De Jong, R., Bergeron, E., Riess, A, Bohlin, R. 2006, NICMOS ISR 2006-001, "NICMOS count-rate dependent non-linearity tests using flatfield lamps"

Fixen, D. J., et al. 2000, PASP, 112, 1350

Gilliland, R., 2004, ACS ISR 2004-01, "ACS CCD Gains, Full Well Depths, and Linearity up to and Beyond Saturation"

Hilbert, B, 2008, WFC3 ISR 2008-39, "WFC3 TV3: Testing: IR Channel Nonlinearity correction"

Hilbert, B and McCullough, P., 2009, WFC3 ISR 2009-21, "WFC3 SMOV Results: IR Channel Dark Current, Readnoise, and Background Signal"

Riess, A., 2010, WFC3 ISR 2010-07, "First On-orbit Measurements of the WFC3-IR Count-rate Non–Linearity"

Smith, R., Zavodny, M., Bonati, M. and Rahmer, G., 2007, SPIE NSS2007, "Image Persistence in 1.7 micron cut-off HgCdTe Focal Plane Arrays for SNAP"